Feasibility of Noninvasive Measurement of Deep Brain Temperature in Newborn Infants by Multifrequency Microwave Radiometry

K. Maruyma, S. Mizushina, *Member, IEEE*, T. Sugiura, *Member, IEEE*, G. M. J. Van Leeuwen, J. W. Hand, G. Marrocco, *Member, IEEE*, F. Bardati, *Member, IEEE*, A. D. Edwards, D. Azzopardi, and D. Land

***Abstract*—Clinical studies of hypothermal neural rescue therapy for newborn infants who have suffered hypoxia-ischaemia are currently hindered by the difficulty in measuring deep brain temperature. This paper addresses: the specific requirements for this measurement problem, the design of a proposed radiometer system, a method for retrieving the temperature profile within the cooled head, and an estimation of the precision of the measurement of deep brain temperature using the technique. A five-frequency-band radiometer with a contact-type antenna operating within the range 1–4 GHz is proposed to obtain brightness temperatures corresponding to temperature profiles predicted by a realistic thermal model of the cooled baby head. The problems of retrieving the temperature profile from this set of brightness temperatures, and the estimation of its precision, are solved using a combination of model fitting and Monte Carlo techniques. The results of this paper show that the proposed technique is feasible, that it is expected to provide a good estimate of the temperature profile within the cooled baby-head, and that the estimated precision (2σ) of the temperature measured in the deep brain structures is better than 0.8 K, depending upon the estimation procedure used.**

***Index Terms*—Biomedical monitoring, brain cooling, hypothermia, microwave radiometry, neural rescue, noninvasive temperature measurement, pediatrics.**

I. Introduction

STUDIES OF experimental cerebral injury have shown that promoting or allowing moderate cooling of the brain after hypoxia-ischaemia can reduce damage and improve functional outcome [1], [2]. The mechanism of neuroprotection is unclear, but mild hypothermia (33 °C–35 °C): 1) reduces the fall in PCr/Pi seen during delayed injury in immature piglets and rats [3]; 2) suppresses the development of delayed cytotoxic oedema in fetal sheep [4]; 3) reduces extracellular concentrations of excitatory amino acids [5]; and 4) reduces the number of cells with the characteristics of apoptosis in newborn piglets [6]. The simplicity of hypothermic neural protection has already led to preliminary clinical trials of moderate cooling in newborn infants suffering perinatal asphyxia [7], [8]. However, there are few data available on the temperature distribution within the newborn brain, or on the effect of either local or systemic cooling. Accurate invasive measurements of newborn infant brain temperature cannot easily be justified, and animal models may be misleading due to differences in cerebral metabolism, blood flow, or geometry. However, successful clinical application of brain cooling requires that, as with any other therapy, the dose distribution of cooling is known. This is particularly important, as studies using magnetic resonance imaging (MRI) have demonstrated that, in newborn infants, not only are the basal ganglia significantly warmer than more superficial cerebral tissues [9]–[12], but injury to the deep brain structures predicts severe neurological impairment, while cortical injury is relatively benign.

MRI and magnetic resonance spectroscopy (MRS) methods have been used to measure temperature changes in the brain [9], [13], [14]. However, these require access to complex equipment, and they are not suitable for routine measurements repeated over a prolonged period of time. They may, however, have value in validating other methods.

A possible alternative method for noninvasive temperature sensing and monitoring that is completely passive and inherently safe is microwave radiometry (MWR). It has been used in a variety of diagnostic medical applications [15]–[17], including the investigation of intracranial thermogenic or ischaemic regions associated with tumors or vascular lesions [18].

MWR involves measuring the power in the microwave region of the natural thermal radiation from body tissues to obtain the brightness temperature of the tissue under observation. The brightness temperature $T_{B,i}$ may be defined as

$$T_{B,i} = \frac{P_i}{k\Delta f_i} = \frac{(1-R_i)P_{\text{tissue},i}}{k\Delta f_i} = (1-R_i)T_{B,\text{tissue},i} \tag{1}$$

where $P_{\text{tissue},i}$ is the thermal radiation power emitted by the tissue, P_i is the power received by the antenna in a bandwidth

Manuscript received November 24, 1999; revised February 20, 2000. This work was supported in part by the U.K. Engineering and Physical Sciences Research Council (EPSRC) under a grant and by the Garfield Weston Foundation under a grant.

K. Maruyma and T. Sugiura are with the Research Institute of Electronics, Shizuoka University, Hamamatsu, Shizuoka 432-8011, Japan.

S. Mizushina was with the Research Institute of Electronics, Shizuoka University, Hamamatsu, Shizuoka 432-8011, Japan. He is now with the Telecommunications Advancement Organization of Japan Hamamatsu Lifeline Research Center, Hamamatsu, Shizuoka 432-8061, Japan.

G. M. J. Van Leeuwen and J. W. Hand are with Radiological Sciences Unit, Department of Imaging, Imperial College School of Medicine, London W12 ONN, U.K.

G. Marrocco and F. Bardati are with Dipartimento di Informatica, Sistemi e Produzione, Università di Roma 1"Tor Vergata," 00133 Rome, Italy.

A. D. Edwards and D. Azzopardi are with Department of Paediatrics, Imperial College School of Medicine, London W12 ONN, U.K.

D. Land is with Department of Physics and Astronomy, University of Glasgow, Glasgow G12 8QQ, Scotland.

Publisher Item Identifier S 0018-9480(00)09708-8.

Δf_i around a center frequency f_i, R_i is the power reflection coefficient at the skin–antenna interface at f_i, and k is Boltzmann's constant. According to the Rayleigh–Jeans law, at microwave frequencies, the thermal radiation intensity is proportional to the absolute temperature and, thus, $T_{B,i}$ may be expressed as

$$T_{B,i} = \iiint_{afv} W_i(\boldsymbol{r}) T(\boldsymbol{r})\, dv \tag{2}$$

where $T(\boldsymbol{r})$ is the absolute temperature in an incremental volume of tissue dv located at $\boldsymbol{r}$, $W_i(\boldsymbol{r})$ is the radiometric weighting function (WF), and the integration is over the antenna's field of view (afv). Thus, the measured brightness temperature (assuming use of a radiometer operating in the radiation balanced mode [19], [20]) is

$$T_{B,\mathrm{meas},i} = T_{B,\mathrm{tissue},i} = \frac{1}{1-R_i} \iiint_{afv} W_i(\boldsymbol{r}) T(\boldsymbol{r})\, dv \tag{3}$$

and, in general, is dependent upon: 1) the actual temperature distribution throughout the tissues viewed and 2) the receiving antenna's WF, which, in turn, depends upon its operating frequency, dimensions, the permittivity of the material with which it is filled, the microwave attenuating properties of the tissues and any bolus present, and microwave reflections occurring at interfaces between different tissue regions and between these regions and the measuring equipment.

Since both microwave attenuation in tissue and the antenna's characteristics are frequency dependent, the temperature-depth profile within the tissue beneath the antenna can be found by determining a set of $T_{B,\mathrm{meas},i}$ using a multifrequency radiometer and then solving the inverse problem.

II. Measurement Problem

The problem posed is to determine a routine noninvasive direct measurement of the temperature of the diencephalon during topical cooling of the neonatal head. The selected method should be available over prolonged periods since neural protection therapy may involve mild hypothermia being maintained for periods up to 72 h.

Numerical modeling of the temperature distribution within an anatomically realistic simulation of an infant's head and a reduced size adult head has been reported [21]. Sensitivity of the predictions of the model to different rates of cerebral blood flow, variation in the thermal resistance of the skin, and the method of describing heat transport within tissue (heat sink *versus* realistic vascular tree) were examined. Fig. 1 shows the baby head model, derived from MRI data, and predicted temperatures within the cooled head. These results are in general agreement with those from other models [22], [23] and measurements [9]. The results suggest that the temperature profile to be retrieved from the radiometric measurements is characterized by a significant temperature gradient within the most superficial 20 mm of tissue and only small temperature variations at approximately 20–50-mm depth. The maximum depth at which temperature must be retrieved is approximately 50 mm.

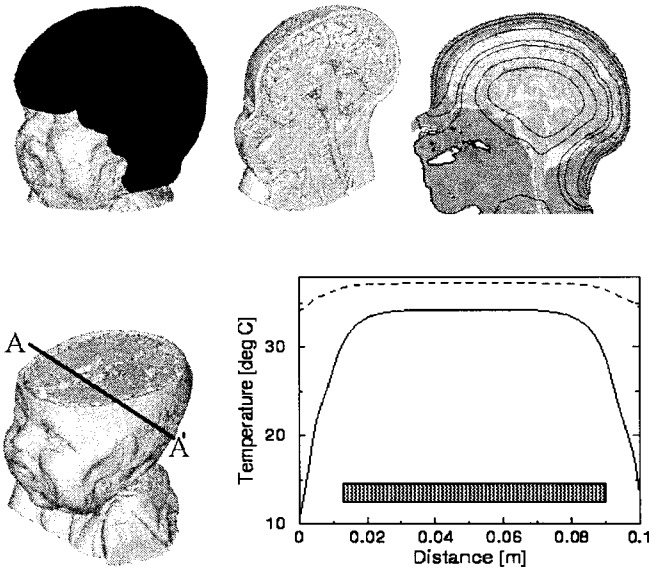

Fig. 1. Anatomically realistic baby head model and predicted temperatures (after [21]). Top: (left)—baby head with cooling cap (dark shading), (center)—sagittal section of model in which isothermal contours were plotted, (right)—contours (from innermost outwards at 34.2 °C, 34 °C, 33 °C, 32 °C, 27 °C, 22 °C, 17 °C, and 12 °C, respectively) in sagittal section assuming heat-sink model, cooling cap at 10 °C, and core temperature of 34 °C, ambient temperature 32 °C. Bottom: (left)—axial section and line for temperature profile, (right)—temperature profile predicted along AA′ assuming the same cooling conditions (lower curve) and no cooling (upper curve). The shaded area represents the presence of brain along the line AA′. Details of the model are given in [21].

III. Hardware Design

A separate Dicke radiometer [24] operating in the radiation balance mode [19], [20] is proposed for each of the five frequency bands. This provides insensitivity to variations in the gain of the radiometer and compensates for power reflections at the tissue/antenna interface, enabling the brightness temperature to be determined independently of the reflection coefficient. The proposed radiometer system is shown schematically in Fig. 2.

The use of low-noise high-gain amplifiers ($\leq$1-dB noise figure, 36-dB power gain), together with a bandwidth of 0.4 GHz and a measurement integration time of 5 s will result in a theoretical brightness temperature resolution of 0.04 K for each radiometer. The brightness temperature resolution achievable with the proposed design (0.04 K) is close to the theoretical value (0.036 K), compared with $\approx$0.07 K for an earlier design, in which only two receivers (1–2 and 2–4 GHz) and one reference noise source were used and local oscillators were connected to the mixers consecutively [25].

A single dual-polarized rectangular waveguide antenna filled with high-permittivity ($\varepsilon_r = 60$) low-loss material will be used to cover the entire frequency range.

A temperature controller adjusts the temperature of the reference noise sources to maintain zero output at the lock-in detectors. To minimize systematic errors, the coaxial cables connecting the antenna to the radiometers will be thermally insulated and temperature monitored, and the temperatures of the p-i-n switches and receiver housings will also be stabilized. The temperature of the antenna will be maintained at the surface temperature of the head under investigation.

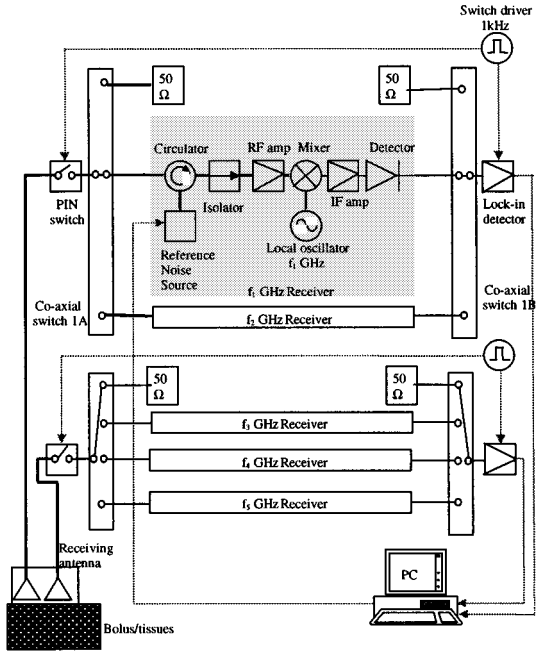

Fig. 2. Proposed five-band microwave radiometer. A single cross-polarized antenna is used to cover 1-4 GHz in 1–2- and 2–4-GHz bands. Two receivers (center frequencies f_1, f_2 GHz) cover the first and three receivers (center frequencies f_3, f_4, f_5 GHz) cover the second of these bands. The receivers are connected sequentially to the appropriate connection on the antenna by means of multithrow coaxial switches. All receivers are switched at a rate of 1 kHz between individual reference noise sources and the bolus/tissues. The reference noise sources are adjusted to maintain zero output from the lock-in detectors.

TABLE I
DIELECTRIC PROPERTIES OF THE BRAIN, CSF, SKULL FOR NEWBORN INFANT'S HEAD, DEIONIZED WATER IN THE BOLUS, AND DIELECTRIC FILLING FOR THE WAVEGUIDE ANTENNA

Material	Permittivity ε_r Conductivity σ (S/m)	Center Frequency f_i (GHz) 1.2	1.65	2.3	3.0	3.6
Brain	ε_r	53.83	53.09	52.13	51.22	50.56
	σ	1.45	1.67	2.05	2.54	3.03
CSF	ε_r	64.83	64.49	63.81	62.85	61.83
	σ	1.64	2.09	2.61	3.01	3.22
Skull	ε_r	8.01	8.03	8.02	7.97	7.89
	σ	0.12	0.14	0.18	0.22	0.26
De-ionized Water	ε_r	84.33	84.29	83.76	82.58	81.06
	σ	0.41	0.76	1.40	2.28	3.20
Dielectric Filling	ε_r	60.00	60.00	60.00	60.00	60.00
	σ	0	0	0	0	0

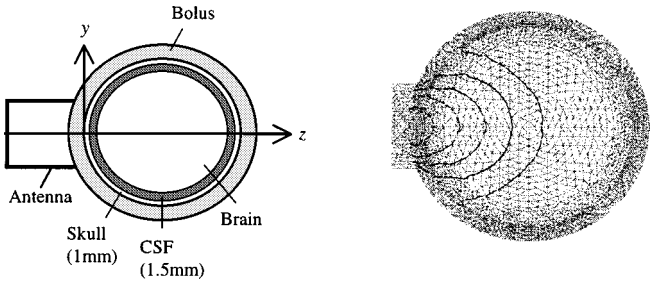

Fig. 3. WF obtained by the FEM for a circular cylindrical model of the baby's head at 1.2 GHz. Diameter of head: 10 cm. Skull: 1 mm. CSF: 1.5 mm. The power loss distribution (power loss density)/(input power) values shown in the right-hand-side figure are (from antenna outwards): $10^{-2.5}$, 10^{-3}, $10^{-3.5}$, 10^{-4}, and $10^{-4.5}$ cm^{-3}.

IV. TEMPERATURE RETRIEVAL

A. WF

1) Derivation: From the definition of brightness, temperature, and the application of the reciprocity theorem to the antenna, the radiometric WF can be expressed as

$$\frac{W_i(\boldsymbol{r})}{1-R_i} = \frac{(1/1)\sigma|E(\boldsymbol{r})|^2}{\iiint\limits_{afv} (1/2)\sigma|E(\boldsymbol{r})^2\, dv} \tag{4}$$

where E is the electric-field intensity induced in tissue by the antenna operated in the active mode [26]. When the geometry and dielectric properties of tissue, the deionized water bolus and dielectric filling for antenna are given, the WF can be derived numerically. In this paper, a two-dimensional (2-D) model consisting of the skull, cerebrospinal fluid (CSF), and brain is used to represent the baby's head. Dielectric properties of the brain (mixture of gray and white matters), CSF, skull, deionized water, and dielectric filling for antenna used in this paper are listed in Table I [27]–[33].

The WF obtained for a circular cylindrical model with a 10-cm diameter, skull (1 mm), CSF (1.5 mm), and brain calculated using a finite-element method (FEM) at 1.2 GHz are shown in Fig. 3. The WFs obtained for the 2-D realistic head model by a 2-D analysis using the finite-difference time-domain (FDTD) technique at 1.2, 1.65, 2.3, 3.0, 3.6 GHz are presented in Fig. 4.

2) Reduction to One-Dimensional Problem: Referring to the temperature contours and profiles shown in Fig. 1, the three-dimensional (3-D) temperature field in the head under external cooling can be approximated by isomorphic iso-temperature shells [34]. To represent these iso-temperature shells by a simplified model, the following two types of approximation are considered here: 1) a concentric cylinder approximation and 2) a plane-parallel approximation, as shown in Fig. 5(a) and (b), respectively. The concentric cylinder approximation may be suitable for use with the 2-D cylindrical head model. The iso-temperature contours in the realistic 2-D head section are approximately ovals. Since these contours run approximately parallel to the aperture and the WFs drop to relatively low values far from the axis of the antenna in the evaluation of the brightness temperatures, a plane-parallel approximation for the iso-temperature contours may be worth considering.

The temperature can then be expressed as a function of a single z-parameter, where z is the distance from surface along the axis of antenna field of view with its origin at the bolus–head surface interface. Thus, surface integration over the iso-temperature shells leads to

$$T_{B,\mathrm{tissue},i} = \iiint\limits_{afv} \frac{W_i(\boldsymbol{r})}{1-R_i} T(\boldsymbol{r})\, dv = \int_{afv} \frac{W_i(z)}{1-R_i} T(z)\, dz \tag{5}$$

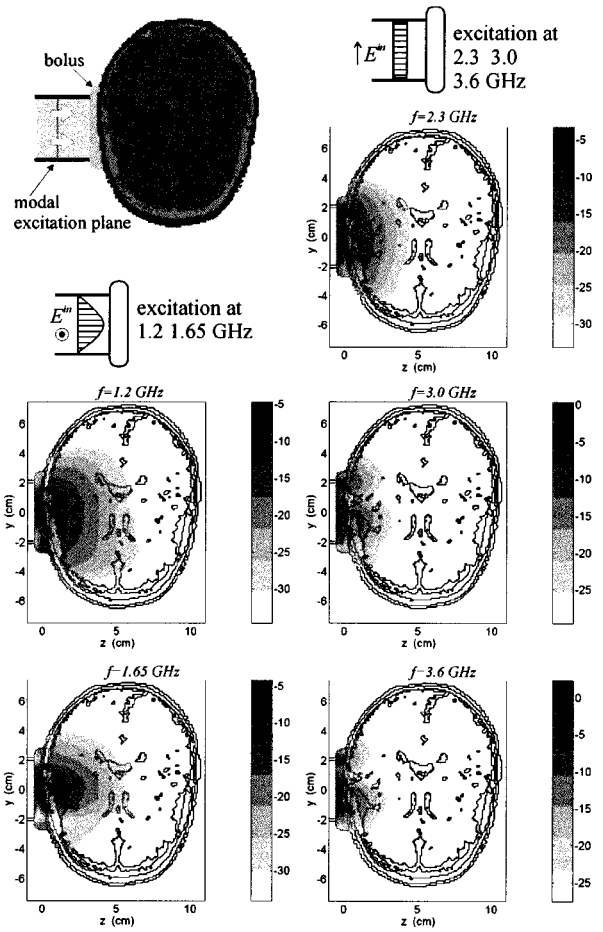

Fig. 4. WFs for a 2-D realistic model of baby's head obtained by a 2-D analysis using FDTD at 1.2, 1.65, 2.3, 3.0, and 3.6 GHz. The shading of the WFs is on a decibel scale.

with

$$\frac{W_i(z)}{1-R_i} = \iint_S \frac{W_i(\boldsymbol{r})}{1-R_i}\, dS. \tag{6}$$

The function $W_i(z)/(1-R_i)$, thus defined, is called the one-dimensional (1-D) WF, where S refers to the surface of equal temperature. The 1-D WFs computed for the cylindrical head model with concentric cylinder approximation and the realistic head model with plane-parallel approximation are presented in Fig. 6(a) and (b), respectively.

B. Temperature Profile Model Function

To retrieve the temperature profile from the radiometric measurement data, we introduce a temperature profile model function. A model function of the form [35]

$$\begin{aligned} T_{\text{model}}(z) &= T_W, \qquad l_b \le z < 0 \\ T_{\text{model}}9z) &= T_0 + \Delta T\{\exp(-z/a) - \exp(-z/b)\}, \qquad 0 \le z \end{aligned} \tag{7}$$

is used, where l_b is the thickness of bolus. In the above expression, T_W, T_0 are the temperature of bolus water and of surface of the baby's head, respectively, while the ΔT term represents the gradual increase of temperature toward the center of the head. Essentially, ΔT, a, and b determine the magnitude of temperature elevation above T_0, the curvature near surface and the position of temperature peak, respectively.

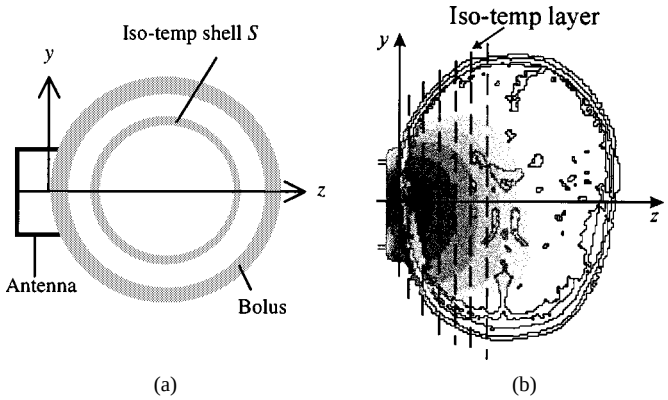

(a) (b)

Fig. 5. Simplified iso-temperature shell models for the temperature field in cooled baby's head. (a) 2-D cylindrical head model with the concentric cylinder approximation. (b) Realistic 2-D head model with the plane-parallel approximation.

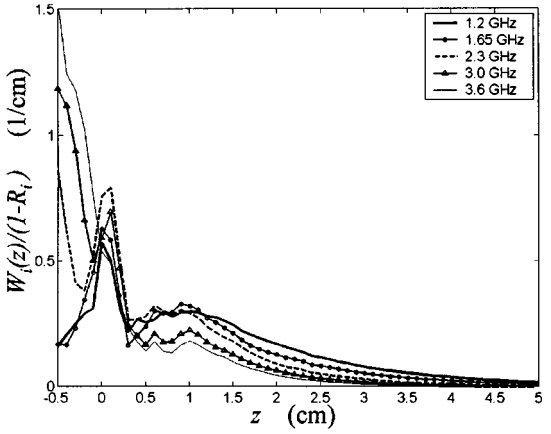

(a)

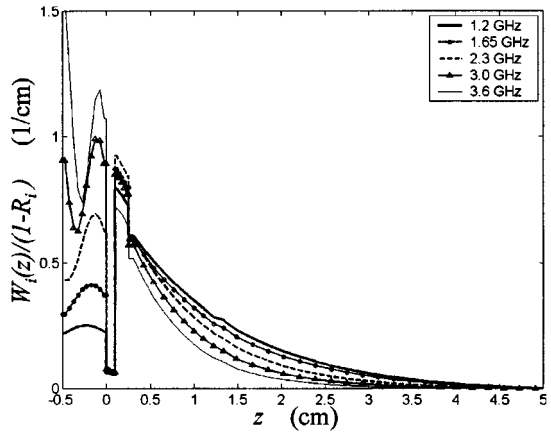

(b)

Fig. 6. 1-D WFs for: (a) circular cylindrical head model with the concentric cylinder approximation [see Fig. 5(a) and (b)] realistic head model with the plane-parallel approximation [see Fig. 5(b)].

C. Model Fitting

First, the brightness temperatures for the model $T_{B,\mathrm{model},i}$ are computed at the measurement frequencies by numerical integration over $T_{\mathrm{model}}(z)$. The result can be written as

$$\int_{afv} \frac{W_i(z)}{1-R_i} T_{\mathrm{model}}(z)\, dz = T_{B,\mathrm{model},i}(T_W, T_0; \Delta T, a, b). \tag{8}$$

Of the five model parameters, T_W, T_0 are determined by probe measurements and are considered as known, while the three remaining parameters ΔT, a, and b are unknown.

1) Three-Parameter Estimation: The three unknown parameters can be determined by fitting the model to radiometric measurements. This is achieved by finding a set of $(\Delta T, a, b)$ that minimizes the error function

$$\mathrm{Error}(\Delta T, a, b) = \sum_{i=1}^{n} \left[T_{B,\mathrm{model},i}(T_W, T_0; \Delta T, a, b) - T_{B,\mathrm{meas},i}\right]^2 \tag{9}$$

where n is the number of radiometric channels.

2) Two-Parameter Estimation: When it is further assumed that the temperature profile has a peak at z_{ctr}, i.e., the center of head, a and b are no longer independent [34] and

$$z_{\mathrm{ctr}} = \frac{a \ln(a/b)}{(a/b) - 1}. \tag{10}$$

Consequently, the number of independent parameters to be determined from the radiometric measurements is reduced to two, namely, ΔT and a/b. This helps to improve the precision of brain temperature retrieval as will be discussed in the following sections.

3) One-Parameter Estimation: If the shape of temperature profiles can be predicted accurately, e.g., from a thermal analysis as in this paper, the shape parameter a/b can be found by fitting the temperature profile model function (7) directly to the profile obtained by the thermal analysis. In this case, ΔT is the only parameter to be determined from radiometric measurements. Elimination of shape parameters from the parameter-estimation procedure is quite effective in improving the precision of the temperature measurement since small changes in the exponent induce large changes in the estimated temperature.

D. Confidence Interval

The above procedures enable the determination of a temperature profile that fits the set of n-channel radiometric data. Since data fluctuate randomly, so do the estimated profiles. The propagation of random fluctuations from the data to the profile is analyzed by a Monte Carlo technique [26]. Data obtained in each radiometer channel are assumed to have a normal distribution. The mean and standard deviation of the distribution are estimated by an average of $T_{B,\mathrm{meas},i}$ and the resolution of brightness temperature for the channel, respectively. The brightness temperature resolution is expected to be at about 0.04 K for the proposed design, as stated in Section I. It is then possible to estimate the confidence interval as a function of z using the Monte Carlo technique.

TABLE II
SIMULATED BRIGHTNESS TEMPERATURES, TB, SIML, FOR THE PROFILE A OF FIG. 1. TWO SETS OF $W_i(z)$ ARE USED: ONE DERIVED WITH THE CONCENTRIC CYLINDER APPROXIMATION AND THE OTHER DERIVED WITH THE PLANE-PARALLEL APPROXIMATION

$W_i(z)$	$T_{B,siml,i}$ (°C)				
	f_i (GHz)				
	1.2	1.65	2.3	3.0	3.6
Con Cyl Approx.	23.573	22.122	19.829	17.695	15.851
Plane-Parallel. Approx.	21.992	19.021	17.824	14.935	13.659

Since the number of unknown parameters to be determined from radiometric measurements is one, two, or three, the minimum number of radiometer channels n required is, likewise, one, two, or three. However, the confidence interval can be made narrower by using a value of n that exceeds the minimum number, i.e., n = (minimum number) + m (m = 1, 2, ...) since the constraints imposed on the least square fitting procedure become tighter as m increases. The relative improvement is greatest at $m = 1$, and reduces as m increases. A practical choice would be $m = 2 - 3$ and in the proposed design, n is chosen to be five.

E. Simulation

1) Generation of Simulated Radiometric Data: Simulated radiometric data $T_{B,\mathrm{siml},i}$ were generated from the profiles of Fig. 1 by using (8)

$$T_{B,\mathrm{tissue},i} \rightarrow T_{B,\mathrm{siml},i} = \int_{afv} \frac{W_i(z)}{1-R_i} T_{\mathrm{siml}}(z)\, dz. \tag{11}$$

In (11), $T_{\mathrm{siml}}(z)$ refers to the profiles predicted by the thermal analysis. $T_{B,\mathrm{siml},i}$ obtained for profile A of Fig. 1 are given in Table II.

Simulations of the temperature profile retrieval and 2σ estimation were made using two- [34] and one-parameter estimation procedures. The WFs derived for the realistic head model with plane-parallel approximation were used.

2) Two-Parameter Estimation Procedure: Temperature profiles and 2σ intervals were retrieved from the simulated brightness temperature data given in the bottom row of Table II, using the two-parameter estimation procedure described in the previous section. Results are presented in Fig. 7(a). The fit is better in superficial regions than in deep regions, reflecting the characteristics of the WFs and the measured T_0. Estimated temperature at the center of the head was higher than the original data by about 1.5 K and 2σ interval was about 0.8 K for profile A of Fig. 1.

3) One-Parameter Estimation Procedure: First, the temperature profile model function (7) was fitted to the temperature profile A of Fig. 1 to estimate a/b using the least square fitting method. With the aid of (10) and z_{ctr} = 5 cm, a and b were then determined. Results are given in Table III.

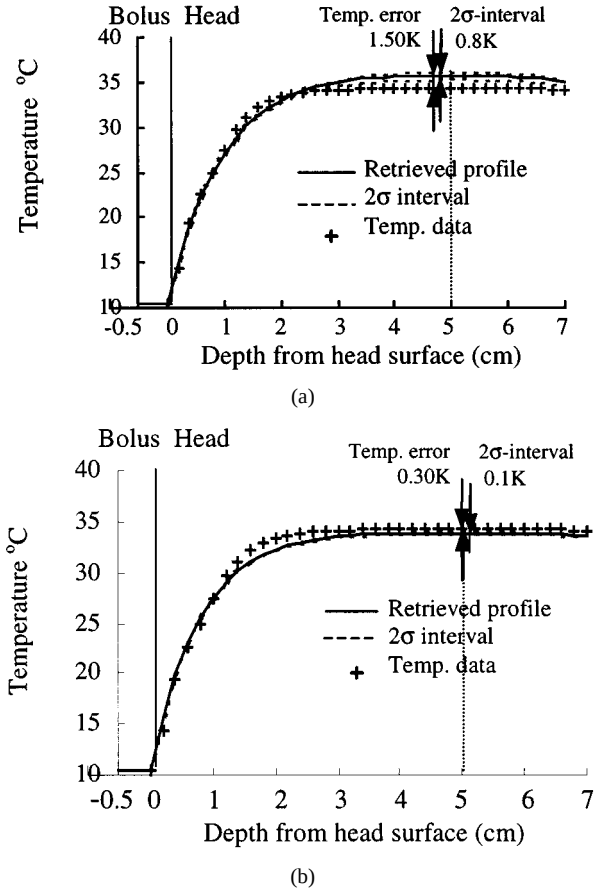

Fig. 7. Temperature profiles (realistic head model) retrieved from $T_{B,\mathrm{siml},i}$, given in the bottom row of Table II and 2σ intervals estimated for these profiles. $T_{B,\mathrm{siml},i}$ are obtained from profile A of Fig. 1. (a) Two-parameter estimation procedure. (b) One-parameter estimation procedure.

TABLE III
SHAPE PARAMETERS OF THE TEMPERATURE PROFILE MODEL FUNCTION FITTED TO PROFILE A OF FIG. 1

$a/b = 542$	
a (cm)	b (cm)
429.7	0.79

Temperature profiles and 2σ intervals were retrieved from $T_{B,\mathrm{siml},i}$ given in the bottom row of Table II using the values of shape parameters given in Table III. Results are presented in Fig. 7(b). Deviation of estimated temperature from original data at the center of the head was 0.3 K and the 2σ interval was 0.1 K.

These results indicate that, with the aid of prediction by thermal analysis, the one-parameter estimation method is promising for accurate and precise noninvasive measurement of deep brain temperature in newborn infants.

V. DISCUSSION

The 2σ-interval values predicted for the retrieved temperature over depths from approximately 30 to 50 mm are typically up to 0.8 K. These predicted values assume realistic noise levels in the radiometer receiver components, a practical averaging time of 5 s per measurement at each frequency, accurate determination of the WFs and both *a priori* knowledge of, and a simple parametric form for, the temperature distribution. The dielectric properties used in this paper were obtained after averaging the literature data for adult humans [28]–[32] and then accounting for the effect of the higher water content of neonatal tissues [27]–[29].

However, the sensitivity of the resultant WFs on changes in tissue dielectric properties and their distribution remains to be performed, although some data are available in the literature [36]. The choice of frequencies used in the present feasibility study is based on adequate coverage of the 1–2- and 2–4-GHz ranges and initial studies based on planar and concentric spherical models. Accurate WFs need to be calculated in the full 3-D model of the head and the set that maximizes spatial differences between WFs determined. Our initial calculations of these 3-D WFs carried out at the lower end of the frequency range are in agreement with the simple 2-D WFs presented herein.

The concept of iso-temperature shells introduced in Section IV-A.2 is firmly based on the results of thermal modeling. This concept leads to the approximation of replacing $T(\boldsymbol{r})$ by $T(z)$ as previously discussed, even though $T(\boldsymbol{r})$ is not separable. The most important consequence of this approximation is the derivation of 1-D WFs from 3-D WFs, as given by (6). This step involves further approximation in the numerical computation in this paper, but more accurate numerical computation is currently underway to arrive at accurate 1-D WFs. In addition, another challenging task is how to best represent the temperature profile by a few parameters. In this feasibility study, we have taken simple one- and two-parameter models to represent the temperature profile. This strategy has had some success in representing temperature data predicted in [21], as shown in Fig. 7. However, since the deviation of the retrieved temperatures from the corresponding assumed values exceeds 1σ at depths from 25 to 50 mm, an alternative parametric description of the temperature profile to be determined may take better advantage of the relatively small 2σ interval.

VI. CONCLUSION

The results of this feasibility study of noninvasive measurement of deep brain temperature in newborn infants by multifrequency MRW show that the proposed technique is expected to provide an acceptable estimate of the temperature profile within the cooled baby head. The proposed design includes a five-frequency-band radiometer with a contact-type antenna operating within the 1–4-GHz range. Retrieval of the temperature profile and an estimate of its precision from the set of brightness temperatures is achieved using a combination of model fitting and Monte Carlo techniques. The estimated 2σ interval at the center of head is better than 0.8 K. In the 2-D models presented, the deviation between the retrieved and initial assumed temperatures was as high as 1.5 K.

Future work will include the determination of 3-D WFs, investigation of alternative parametric descriptions of the temperature profile within the cooled baby head, and the experimental demonstration of the capabilities of this technique.

REFERENCES

[1] F. Colbourne and D. Corbett, "Delayed postischemic hypothermia: A six month survival study using behavioral and histological assessments of neuroprotection," *J. Neurosci.*, vol. 15, pp. 7250–7260, 1995.

[2] E. Sirimanne, R. M. Blumberg, D. Bossano, M. Gunning, A. D. Edwards, P. D. Gluckman, and C. E. Williams, "The effect of prolonged modification of cerebral temperature on outcome following hypoxic-ischaemic brain injury in the infant rat," *Pediatric Res.*, vol. 39, no. 4, pp. 591–597, 1996.

[3] M. Thoresen, J. Penrice, A. Lorek, E. Cady, M. Wylezinska, V. Kirkbride, C. Cooper, G. C. Brown, A. D. Edwards, J. S. Wyatt, and E. O. R. Reynolds, "Mild hypothermia following severe transient hypoxia-ischaemia ameliorates delayed cerebral energy failure in the newborn piglet," *Pediatric Res.*, vol. 37, pp. 667–670, 1995.

[4] C. E. Williams, A. J. Gunn, C. Mallard, and P. D. Gluckman, "Outcome after ischemia in the developing sheep brain: An electroencephalographic and histological study," *Annu. Neurol.*, vol. 31, pp. 14–21, 1992.

[5] M. Thoresen, S. Satas, M. Puka-Sundvall, A. Whitelaw, A. Hallestrom, E. Loberg, U. Ungerstedt, P. A. Steen, and H. Hagberg, "Post-hypoxic hypothermia reduces cerebrocortical release of NO and excitotoxins," *Neuroreport*, vol. 8, pp. 3359–3362, 1997.

[6] A. D. Edwards, X. Yue, M. V. Squier, M. Thoresen, E. B. Cady, J. Penrice, C. Cooper, J. S. Wyatt, E. O. R. Reynolds, and H. Mehmet, "Specific inhibition of apoptosis after cerebral hypoxia-ischaemia by moderate post-insult hypothermia," *Biochem. Biophys. Res. Commun.*, vol. 217, no. 3, pp. 1193–1199, 1995.

[7] A. J. Gunn, P. D. Gluckman, and T. R. Gunn, "Selective head cooling in newborn infants after perinatal asphyxia: A safety study," *Pediatrics*, vol. 102, no. 4, Pt. 1, pp. 885–892, Oct. 1998.

[8] D. Azzopardi, F. M. Cowan, N. J. Robertson, and A. D. Edwards, "Mild whole body hypothermia following birth asphyxia," *Pediatric Res.*, vol. 45, p. 908, 1999.

[9] E. B. Cady, P. C. D'Souza, J. Penrice, and A. Lorek, "The estimation of local brain temperature by *in vitro* $1H$ magnetic resonance spectroscopy," *Mag. Reson. Med.*, vol. 33, pp. 862–867, 1995.

[10] P. Mellergard, "Changes in human intracerebral temperature in response to different methods of brain cooling," *Neurosurgery*, vol. 31, pp. 671–677, 1992.

[11] ——, "Monitoring of rectal, epidural, and intraventricular temperature in neurosurgical patients," *Acta Neurochiral Suppl. Wien.*, vol. 60, pp. 485–487, 1994.

[12] ——, "Intracerebral temperature in neurosurgical patients: Intracerebral temperature gradients and relationships to consciousness level," *Surgical Neurol.*, vol. 43, no. 1, pp. 91–95, Jan. 1995.

[13] R. J. Corbett, A. R. Laptook, G. Tollefsbol, and B. Kim, "Validation of a noninvasive method to measure brain temperature *in vivo* using $1H$ NMR spectroscopy," *J. Neurochem.*, vol. 64, pp. 1224–1230, 1995.

[14] J. R. MacFall, D. M. Prescott, H. C. Charles, and T. V. Samulski, "$1H$ MRI phase thermometry *in vivo* in canine brain, muscle, and tumor tissue," *Med. Phys.*, vol. 23, pp. 1775–1782, 1996.

[15] D. V. Land, "A clinical microwave thermography system," *Proc. Inst. Elect. Eng.*, vol. 134A, pp. 193–200, 1987.

[16] S. Mizushina, *Non-Invasive Temperature Measurement*. New York: Gordon and Breach, 1989.

[17] Y. Leroy, B. Bocquet, and A. Mamouni, "Non-invasive microwave radiometry thermometry," *Physiol. Meas.*, vol. 19, no. 2, pp. 127–148, May 1998.

[18] P. Thouvenot, J. Robert, A. Mamouni, and C. Renard, "Microwave thermometry in intracranial pathology," in *Biomed. Thermol.*, M. Gautherie and E. Albert, Eds. New York: Alan Liss, 1982, pp. 501–508.

[19] D. F. Wait and T. Nemoto, "Measurement of the noise temperature of a mismatched noise source," *IEEE Trans. Microwave Theory Tech.*, vol. MTT-16, pp. 670–675, Sept. 1968.

[20] K. M. Lüdeke, B. Schiek, and J. Kohler, "Radiation balance microwave thermograph for industrial and medical applications," *Electron. Lett.*, vol. 14, pp. 194–196, 1978.

[21] G. M. J. Van Leeuwen, J. W. Hand, A. D. Edwards, D. Azzopardi, and J. J. W. Lagendijk, "Numerical modeling of temperature distributions within the neonatal head," *Pediatric Res.*, vol. 48, no. 3, pp. 351–356, 2000.

[22] D. A. Nelson and S. A. Nunneley, "Brain temperature and limits on transcranial cooling in humans: Quantitative modeling results," *European J. Appl. Physiol.*, vol. 78, pp. 353–359, 1998.

[23] S. A. Xu, P. Tikuisis, and G. Giesbrecht, "A mathematical model for human brain cooling during cold-water near-drowning," *J. Appl. Physiol.*, vol. 86, pp. 265–272, 1999.

[24] R. H. Dicke, "The measurement of thermal radiation at microwave frequencies," *Rev. Sci. Instrum.*, vol. 17, pp. 268–275, 1946.

[25] S. Mizushina, M. Matsuda, K. Matsui, Y. Hamamura, and T. Sugiura, "Non-invasive temperature profiling using multi-frequency microwave radiometry in presence of water-filled bolus," *Trans. IEICE*, vol. E74, pp. 1293–1302, 1991.

[26] S. Mizushina, T. Shimizu, K. Suzuki, M. Kinomura, H. Ohba, and T. Sugiura, "Retrieval of temperature-depth profiles in biological objects from multi-frequency microwave radiometric data," *J. Electromag. Waves Applicat.*, vol. 7, pp. 1515–1548, 1993.

[27] J. Dobbing and J. Sands, "Quantitative growth and development of human brain," *Archives Disease in Childhood*, vol. 48, pp. 757–767, 1973.

[28] K. R. Foster, J. L. Schepps, R. D. Stoy, and H. P. Schwan, "Dielectric properties of brain tissue between 0.01 and 10 GHz," *Phys. Med. Biol.*, vol. 24, pp. 1177–1187, 1979.

[29] J. L. Schepps and K. R. Foster, "The UHF and microwave dielectric properties of normal and tumour tissues: Variation in dielectric properties with tissue water content," *Phys. Med. Biol.*, vol. 25, pp. 1149–1159, 1980.

[30] M. A. Stuchly and S. S. Stuchly, "Dielectric properties of biological substances—Tabulated," *J. Microwave Power*, vol. 15, pp. 19–26, 1980.

[31] C. Gabriel, S. Gabriel, and E. Corthout, "The dielectric properties of biological tissues: I. Literature survey," *Phys. Med. Biol.*, vol. 41, pp. 2251–2269, 1996.

[32] S. Gabriel, R. W. Lau, and C. Gabriel, "The dielectric properties of biological tissues: II. Measurements in the frequency range 10 Hz to 20 GHz," *Phys. Med. Biol.*, vol. 41, pp. 2251–2269, 1996.

[33] J. B. Hasted, *Aqueous Dielectrics*. London, U.K.: Chapman & Hall, 1973, ch. 1, 2, and 3.

[34] K. Maruyama, Y. Niwa, S. Mizushina, J. Hand, H. Hirata, and T. Sugiura, "Non-invasive temperature measurement in neonate's brain using multi-frequency microwave radiometry," in *Proc. Asia–Pacific Microwave Conf.*, vol. 2, 1998, pp. 885–888.

[35] H. Ohba, M. Kinomura, M. Ito, T. Sugiura, and S. Mizushina, "Multi-frequency microwave radiometry for noninvasive thermometry using a new temperature profile model function," *Trans. IEICE Electron.*, vol. E78-C, pp. 1071–1081, 1995.

[36] J. B. Van de Kamer, N. Van Wieringen, A. A. C. De Leeuw, and J. J. W. Lagendijk, "The significance of accurate dielectric tissue data for hyperthermia treatment planning," *Int. J. Hyperthermia*, to be published.

K. Maruyma, photograph and biography not available at time of publication.

S. Mizushina (S'60–M'66), photograph and biography not available at time of publication.

T. Sugiura (M'86), photograph and biography not available at time of publication.

G. M. J. Van Leeuwen, photograph and biography not available at time of publication.

J. W. Hand, photograph and biography not available at time of publication.

G. Marrocco (S'96–M'98), photograph and biography not available at time of publication.

F. Bardati (S'63–M'66), photograph and biography not available at time of publication.

A. D. Edwards, photograph and biography not available at time of publication.

D. Azzopardi, photograph and biography not available at time of publication.

D. Land, photograph and biography not available at time of publication.